Cancer stem cells from human breast tumors are involved in spontaneous metastases in orthotopic mouse models

Huiping Liu[a,b,1,2], Manishkumar R. Patel[c,d,1], Jennifer A. Prescher[c,d,e,1], Antonia Patsialou[f], Dalong Qian[a], Jiahui Lin[a], Susanna Wen[a], Ya-Fang Chang[c,g], Michael H. Bachmann[c,d,e], Yohei Shimono[a], Piero Dalerba[a], Maddalena Adorno[a], Neethan Lobo[a], Janet Bueno[h], Frederick M. Dirbas[i], Sumanta Goswami[f,j], George Somlo[k], John Condeelis[f,2], Christopher H. Contag[c,d,e,2], Sanjiv Sam Gambhir[c,d,l,2], and Michael F. Clarke[a,2]

[a]Institute for Stem Cell Biology and Regenerative Medicine, Stanford University, Palo Alto, CA 94304; [b]Ben May Department for Cancer Research, University of Chicago, Chicago, IL 60637; [c]Department of Radiology, [d]Molecular Imaging Program, and [e]Departments of Pediatrics and Microbiology and Immunology, Stanford University, Stanford, CA 94305; [f]Department of Anatomy and Structural Biology, Albert Einstein College of Medicine, Bronx, NY 10461; [g]Department of Biomedical Imaging and Radiological Sciences, National Yang-Ming University, Taipei, Taiwan 112; Departments of [h]Pathology and [i]Surgery, Stanford University, Stanford, CA 94305; [j]Department of Biology, Yeshiva University, New York, NY 10033; [k]City of Hope Cancer Center, Duarte, CA 91010; and [l]Department of Bioengineering, Stanford University, Stanford, CA 94305

Edited* by Janet D. Rowley, University of Chicago, Chicago, IL, and approved September 14, 2010 (received for review May 26, 2010)

To examine the role of breast cancer stem cells (BCSCs) in metastasis, we generated human-in-mouse breast cancer orthotopic models using patient tumor specimens, labeled with optical reporter fusion genes. These models recapitulate human cancer features not captured with previous models, including spontaneous metastasis in particular, and provide a useful platform for studies of breast tumor initiation and progression. With noninvasive imaging approaches, as few as 10 cells of stably labeled BCSCs could be tracked in vivo, enabling studies of early tumor growth and spontaneous metastasis. These advances in BCSC imaging revealed that $CD44^+$ cells from both primary tumors and lung metastases are highly enriched for tumor-initiating cells. Our metastatic cancer models, combined with noninvasive imaging techniques, constitute an integrated approach that could be applied to dissect the molecular mechanisms underlying the dissemination of metastatic CSCs (MCSCs) and to explore therapeutic strategies targeting MCSCs in general or to evaluate individual patient tumor cells and predict response to therapy.

breast cancer | human-in-mouse cancer models | fused optical reporters | bioluminescence imaging

Cancer stem cells (CSCs) were first identified in human leukemia (1, 2) and exhibited capacity to form tumors in immunodeficient mice. Because CSCs are characterized from various types of cancers, CD44 has been a useful marker for enriching CSCs not only for breast tumors but also a variety of other epithelial tumor models (3–17). We and others have previously reported that CSCs are more resistant to traditional cancer therapies (4, 18, 19). There is circumstantial evidence that CSCs may be involved in metastasis of solid tumors, including breast cancer. Breast CSCs (BCSCs) possess an "invasiveness" gene signature that correlates with poor overall survival and shortened metastasis-free survival in cancer patients (20). Importantly, BCSCs are enriched for cells that can undergo epithelial–mesenchymal cell transition (EMT), which likely plays a critical role in metastases in at least some tumors (21). The observation that microRNAs in normal breast stem cells and BCSCs can regulate both EMT and self-renewal further suggests that CSCs might somehow play a role in metastasis (22). Nonetheless, there remains uncertainty surrounding the contributions of CSCs to metastasis.

Understanding the role of CSCs in metastasis requires a reliable, noninvasive measure of BCSC outgrowth and dissemination in representative and predictive models of human metastatic disease. Because of genetic differences in mouse tumors or genetic changes that occur with establishment of cell lines, the commonly used models to study metastases, including those involving human cancer cell lines, mouse tumor models, and/or metastatic tumor models via bloodstream injections, do not fully recapitulate human disease (9, 23–25). Here, by implanting patient tumors or BCSCs into mouse mammary fat pads and using noninvasive imaging strategies, we established representative human-in-mouse orthotopic xenograft tumor models that developed spontaneous metastases. The BCSCs were tagged through expression of optical bifusion reporter genes to facilitate their visualization in the living mouse, enable their retrieval for subsequent flow cytometry and functional analyses, and guide the selection of cells for ex vivo or in vivo analysis and/or killing assays. Several early-passage xenograft tumors were identified in which the growth and dissemination of BCSCs could be monitored using noninvasive imaging techniques. The collection of live invasive cells from the primary tumors by use of an in vivo invasion assay (26) enabled phenotypic analysis of the invasive cells in these tumor models. By this approach, we observed an enrichment of the $CD44^+$ population among the invasive breast cancer cells.

Optical imaging approaches that use multifunctional reporter genes permit thorough analyses of disease models by linking in vivo and ex vivo assays and guiding the experimental design (27–32). Such reporters include firefly luciferase (Luc) for whole-body tracking of cells via bioluminescence imaging (BLI) (33) and fluorescent proteins that facilitate intravital imaging and ex vivo analyses (e.g., fluorescence microscopy and flow cytometry). Dual-function BLI-fluorescent reporter constructs constituting the Luc coding sequence fused to that of fluorescent proteins were used to label BCSCs. To maximize the BLI detection sensitivity of BCSCs, we used a modified, codon-optimized version of Luc, Luc2 (34). Cells expressing this reporter were 10–100 times brighter than those with previously reported versions of Luc (Luc^+) (*SI Materials and Methods*). In addition to the widely used enhanced GFP (*eGFP*), we also fused *Luc2* to the red fluorescent protein td-Tomato (*Tom*) (35), which has improved detection

Author contributions: H.L., M.R.P., J.A.P., A.P., P.D., S.G., J.C., C.H.C., S.S.G., and M.F.C. designed research; H.L., M.R.P., J.A.P., A.P., D.Q., J.L., S.W., Y.-F.C., N.L., and S.G. performed research; J.A.P., M.H.B., J.B., F.M.D., and G.S. contributed new reagents/analytic tools; H.L., M.R.P., J.A.P., A.P., Y.S., P.D., M.A., S.G., J.C., C.H.C., S.S.G., and M.F.C. analyzed data; and H.L. wrote the paper.

Conflict of interest statement: C.H.C. has financial interest in Caliper LifeSciences, an in vivo imaging company.

*This Direct Submission article had a prearranged editor.

[1]H.L., M.R.P., and J.A.P. contributed equally to this work.

[2]To whom correspondence may be addressed. E-mail: hliu@uchicago.edu, john.condeelis@einstein.yu.edu, ccontag@stanford.edu, sgambhir@stanford.edu, or mfclarke@stanford.edu.

This article contains supporting information online at www.pnas.org/lookup/suppl/doi:10.1073/pnas.1006732107/-/DCSupplemental.

in vivo relative to GFP. We established optimized parameters to transduce primary or passaged BCSCs with lentiviral vectors encoding Luc2-eGFP (L2G) or Luc2-Tom (L2T) fusion genes; thereby as few as 10 cells of labeled BCSCs could be noninvasively visualized at 16 h after implantation, thus greatly enhancing the accuracy and efficiency of tumorigenic assays compared with traditional monitoring of the formation of palpable tumors that takes 3–6 mo. Driven by the ubiquitin promoter, these optical reporters could be stably expressed over a series of tumor passages. More importantly, they enabled the retrieval and detection of invasive tumor cells (ITCs) collected in vivo (26, 36), as well as micrometastases from mouse lungs, which could not be readily detected by the more labor-intensive traditional invasive methods (e.g., H&E staining), therefore facilitating the identification and phenotypic analysis of invasive and metastatic cells. We demonstrated that $CD44^+$ metastatic cancer cells isolated from the lungs were capable of regenerating tumors upon orthotopic transplantation, suggesting a metastatic role for BCSCs.

Our metastatic models, in combination with noninvasive imaging techniques, might be broadly applicable to rapidly stage disease, assess therapeutic responses, guide in vivo cell selection, and facilitate ex vivo analyses, and as such are essential for functional characterization of CSCs and for preclinical studies of therapies that target these cells.

Results

Generation of Human-in-Mouse Breast Cancer Xenograft Models in NOD/SCID Mice. According to gene expression profiling and hormone receptor status of estrogen receptor (ER), progesterone receptor (PR), and human epidermal growth factor receptor 2 (Her2 or ErbB2), breast cancer is traditionally classified into four or five molecular subtypes: ER^+ (luminal A or luminal B, usually $PR^{+/-}$ $Her2^-$), overexpressed Her2 ($Her2^+$, usually ER^-PR^-), negative for ER, PR, and Her2 ($ER^-PR^-Her2^-$, mostly basal-like), and normal-like (37–41). To generate human-in-mouse orthotopic xenograft tumor models representative of these subtypes, we collected fresh specimens from various types of breast cancer patients and then xenotransplanted sliced tumor specimen or sorted $CD44^+$ $lineage^-$ breast cancer cells into mammary fat pads of nonobese diabetic (NOD)/SCID mice as previously described (3). From breast tumor specimens representing each of these subclasses, we generated eight xenograft tumor models, including two ER^+ (E1, E2), two $Her2^+$ (H1, H2), and four triple-negative (TN) tumors (TN1–TN4) (Fig. S1 and Table S1).

Because TN breast cancers exhibit a more aggressive and metastatic phenotype in the clinic (42), we expected that these tumor-derived orthotopic xenografts would have a higher likelihood of metastasizing, and thus we focused primarily on these models for our studies. Using previously described methods (3), we identified tumorigenic populations from two TN early-passage xenograft tumors, which we called TN1 and TN2. In both tumors, $CD44^+$ cells were demonstrated to be tumorigenic, whereas $CD44^-$ cells were not (Fig. S1 and Table S2).

Visualizing 10 BCSCs in Vivo by BLI. To closely monitor BCSC fates and functions in mice, we labeled $CD44^+$ cells from TN1 or TN2 tumors with dual-function reporters comprising the coding sequences of bioluminescent and fluorescent proteins (28–31, 43), which allow for both BLI in vivo and fluorescence imaging ex vivo, along with flow cytometry analyses. We generated several lentiviral constructs, comprising different reporter genes and promoter sequences, and assayed their utility in labeling BSCSs under a variety of conditions (multiplicity of infection, or MOI, of 5–100) (Fig. S2). We found that the ubiquitin promoter-driven L2G or L2T (pFU-L2G/L2T) led to the most efficient or stable labeling and the brightest bioluminescent signals of BCSCs (Fig. S2), with a sensitivity of BLI detection of one cell in vitro (Fig. S3*A*) and minimum of 10 cells in vivo (Fig. 1*A*). Tumor growth was observed from two of four injections of 10 BCSCs (Fig. S3 *B* and *C*), and the label was stable for at least two or three serial transplantations, with 80–90% of the cells maintaining labeling, as determined by flow cytometry (Fig. 1*B*). Importantly, we did not observe a significant change in tumor phenotypes associated with the lentiviral transduction, as revealed by tumor size, histological appearance, and flow cytometry profiles, and there was no infection of residual mouse stromal cells (Fig. S4 *A–D*). We also observed comparable gene expression profiles between sorted $eGFP^+$ tumor cells and the unlabeled tumor cells by real-time PCR of 30 genes (Fig. S4*E*) that have been shown to regulate invasion in vivo in mouse breast tumor models (36).

A

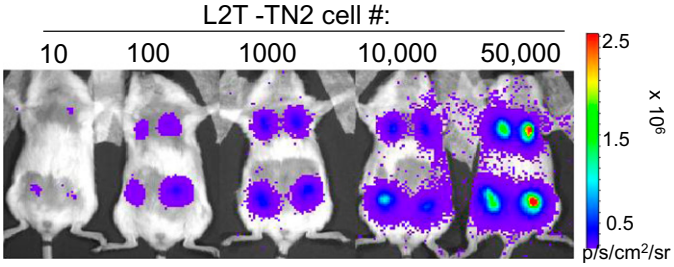

B

Percentage of labeled L2T/L2G cells with the ubiquitin promoter

	parental	p1	p2	p3
L2T	5%	90%	99%	92%
L2G	20%	94%	78%	

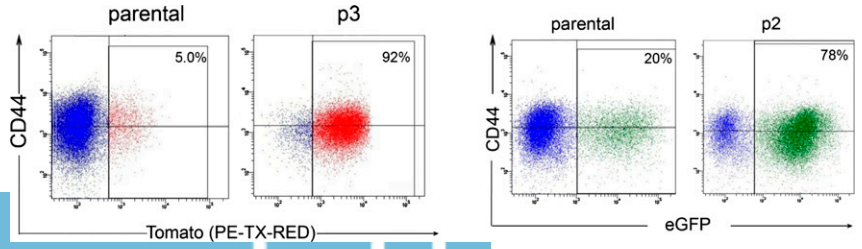

Fig. 1. Visualizing BCSCs with optical reporters. (*A*) BLI of L2T-TN1 tumor cells (10–50,000) implanted into four separate fat pads of NOD/SCID mice. Transduced td-Tomato$^+$ cells were sorted from the labeled parental tumor. (*B*) Stable integration of the optical reporters L2T or L2G into TN1 tumor cells after lentiviral transduction. Reporter expression in harvested cells was measured by flow cytometry in both parental tumors (parental) and passaged tumors (p1–p3). Sample flow cytometry dot plots are shown.

Monitoring the Early Growth of Breast Cancer Cell Subsets in Vivo. On the basis of the 10-cell detection sensitivity enabled by L2G or L2T, we were interested in improving the detection of tumor cell growth in vivo at early time points after implantation, information that is lacking in traditional CSC assays. TN1-BCSCs transduced by L2G (labeled passage 1) were visualized by BLI as early as 16 h after infection/implantation, and their signals intensified over time (Fig. 2 *A* and *B*). Whereas the early cell growth curve was predominantly linear (Fig. 2*B*, *Inset*), the late stage of tumor growth showed an exponential burst of BLI signal that was consistent with the formation of palpable tumors. This finding underscores the utility of BLI in vivo detection methods for monitoring early events in tumorigenesis.

Whereas traditional tumorigenic assays are not amenable to monitoring the cell fate of nontumorigenic cells, we used BLI to more closely evaluate the contributions of different primary cell populations to tumor initiation or progression. We transduced different subsets of primary breast tumor cells from human specimens with L2T or L2G for in vivo implantation and imaging. Both $CD44^+$ and $CD44^-$ human breast cancer cells were transduced by L2T and detected on day 2 after implantation (Fig. 2 *C* and *D*). As shown by the growth curves, $CD44^+$ cells grew at a steady rate over 5 mo. Surprisingly, the signal of $CD44^-$ cells increased slightly after injection but stabilized by day 50–90 and did not increase further over the next 60 d (Fig. 2*D*), indicating that these cells had a limited proliferative capacity. Although these $CD44^-$ tumor cell subsets did not form palpable tumors, BLI provided an efficient and improved method of assessing their proliferation at early time points after implantation in vivo.

Detection of Breast Cancer Metastases in Vivo. Optical imaging enabled the sensitive detection of BCSCs in vivo, suggesting that it could be used to guide the early detection of breast cancer spontaneous metastasis. Using L2G- or L2T-transduced BCSCs, we detected spontaneous lung metastasis of TN1 and TN2 tumors noninvasively in vivo, as well as ex vivo after dissection (Fig. 3*A* and Fig. S5*A*), even though macrometastases were not visually observed within the dissected lung lobules (Fig. S5*B*). We were able to detect lung metastases ex vivo with BLI from all TN1 (n = 53) and TN2 tumor-bearing mice (n = 20) after tumors became 2 to 3 cm in diameter. Furthermore, we detected local lymph node metastases in mice bearing TN1 tumors (Fig. 3*B*) and distant lymph node metastases in mice bearing TN2 tumors (Fig. S5*A*). This indicated that these human-in-mouse orthotopic models represented clinical features of patient tumors with both local and distant metastases. In addition, we labeled E1 ($ER^+PR^+Her^-$) and H2 ($ER^-PR^-Her2^+$) tumor cells with L2T for mouse mammary fat pad implantation and detected spontaneous lung metastases of the E1 tumor-bearing mice with BLI (Fig. S5*C*).

By H&E staining of lung sections, we validated cancer metastases of these breast cancer xenograft models with or without reporter gene transduction (Table S1). The lung and lymph node metastases were confirmed in the labeled TN1 tumor-bearing mouse (Fig. 3*C* and Fig. S6). In addition, by H&E staining lung micrometastases were identified from all four TN xenograft

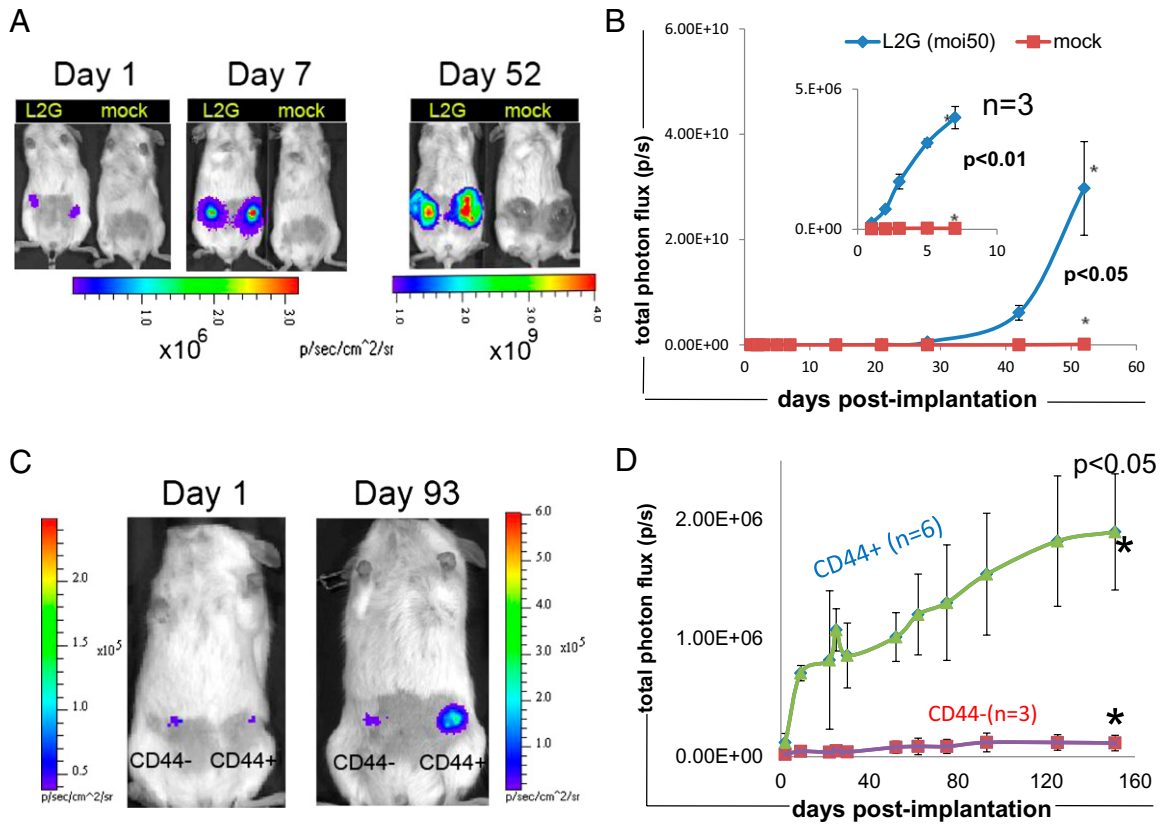

Fig. 2. Analyzing the early growth of breast cancer cell subsets in vivo via BLI. (*A* and *B*) Monitoring tumor growth mediated by TN1 BCSCs (passage 2–5). $CD44^+$ cells (1×10^5) were transduced with L2G (MOI 50) or the mock and then transplanted into mouse mammary fat pads. Mice were imaged from day 1 to day 52 after implantation when palpable tumors formed. Quantification (total flux, photons per second, p/s) of the bioluminescent signal from the tumor regions in *A* is depicted in *B*. Error bars represent the SD of the mean for three experiments. *$P < 0.01$ for early-phase growth curve day 7 and $P < 0.05$ for day 52. (*C* and *D*) Analysis of primary breast tumor cell subsets into NOD/SCID or NSG (NOD/SCID with IL2R-γchain$^{-/-}$) mice. Primary breast tumor cells were dissociated from clinical patient specimens, and 3,000 $CD44^+$ or $CD44^-$ cells were sorted for transduction with L2T fusion reporter gene (MOI 10), implanted into mice, and analyzed by BLI over time. Representative images are shown in *C* and the light emission is quantified in *D*. Error bars represent SD of the mean for six replicate experiments (three from NSG mice).

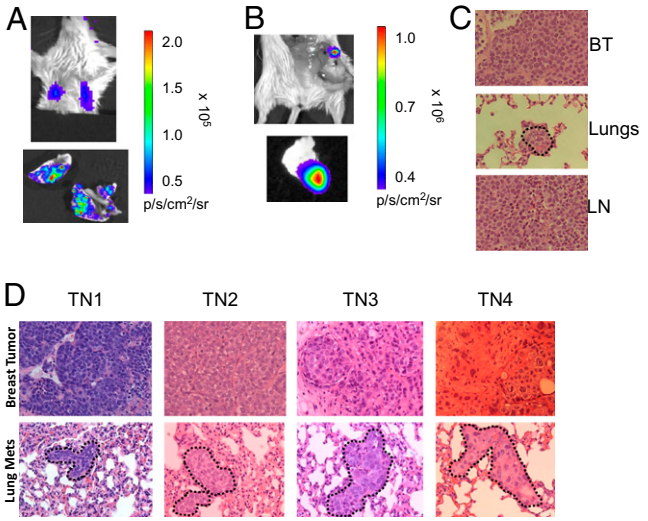

Fig. 3. BLI revealed lung and lymph node metastases. (*A*) Spontaneous lung metastases detected noninvasively in mice bearing a TN1 tumor (passage 3) in the L4 mammary fat pad (*Upper*). Focal metastases were observed throughout the lung upon dissection, placed in a plate with PBS (*Lower*). (*B*) Residual BLI signal observed in the animal after the tumor section (*Upper*) localized to lymph node (*Lower*) (Fig. S6). (*C*) Representative H&E stains of sections from the breast tumor (BT), dissected lungs in *A*, and lymph nodes (LN) in *B*. (Magnification: 200×.) (*D*) Representative H&E stains of sections from four TN tumors (TN1–TN4) and mouse lungs. (Magnification: 200×.)

tumor models (TN1–TN4) (Fig. 3*D*) and E1 tumor models (Fig. S5 *D* and *E*), although lung metastases from some TN1 or E1 mice were missed by limited slides of lung sectioning (Table S1). This underscores the efficiency and sensitivity of BLI in metastasis detection as the imaging technique is used to guide tissue selection for these more labor-intensive assays.

With our spontaneous metastasis models, we wanted to investigate whether BCSCs were directly involved in metastasis, particularly in the initial invasion step. Using an established in vivo invasion assay, whereby migration toward a cytokine gradient can be tested in the primary tumor microenvironment (26, 36), we first demonstrated that tumor cells from both TN1 and TN2 primary breast tumors were invasive and chemotactic to EGF in vivo (Fig. 4 *A* and *B*). Because of the limited numbers of cells we could collect from each tumor, we used a Guava microcapillary flow cytometer to analyze the expression of CD44 on sorted eGFP$^+$ ITCs and average primary tumor cells (APTCs) from the TN1 breast tumors. Compared with APTCs, the ITCs were significantly enriched with CD44^{high} cells (41% of ITCs vs. 17% of total APTCs from this tumor) (Fig. 4 *C* and *D*). These results clearly demonstrated the preferential invasive behavior of the BCSCs in vivo.

Tumorigenic Assays of TN1 and TN2 Metastatic Cancer Cells. To test whether metastatic cancer cells share properties with primary BCSCs, we analyzed the marker expression profiles and tumorigenic capacity of lung metastatic cells isolated from TN1 and TN2 breast cancers. Histological analysis revealed that in both TN1 and TN2 tumor models, lung metastatic cells and primary tumor cells had similar expression patterns of high-molecular-weight cytokeratins (CK34BE12 or CK5/6) and proliferation indexes as assayed by Ki67 levels (Fig. S7*A*). Although metastatic cells were a rare population (0.5–2%) in the lungs (Fig. S7*B*), we took advantage of L2G- or L2T-transduced tumor models for clear identification and guided dissection of human cancer cells from lungs that shared similar expression profile of CD44 with parental breast cancer cells in the primary site (17–30% CD44$^+$ cells) (Fig. 5*A*).

To investigate whether metastatic cells contained BCSCs, we isolated lung cells from unlabeled TN1- or TN2-bearing mice and implanted bulk lung cells into mouse mammary fat pads for tumorigenic assays. The lung metastatic cells regenerated tumors upon implantation into the mammary fat pads (Fig. 5*B*), indicating the existence of BCSCs in the lung micrometastatic lesions. We further analyzed the expression profiles of CD44 in unlabeled lung metastatic cells excluding mouse stromal cells (Fig. 5*B*) and performed tumorigenic assays in vivo with sorted CD44$^+$ and CD44$^-$ populations of TN1 or TN2 lung metastases. CD44$^+$ metastatic cells from either TN1 or TN2 models were more tumorigenic than CD44$^-$ cells upon implantation into orthotopic mammary fat pads of NOD/SCID mice (Fig. 5*B*), and these CD44$^+$ populations isolated from grown tumors were able to passage and differentiate again in mice (Fig. S7*B*). These data implicated the self-renewal and differentiation capacity of CD44$^+$ cells.

Whereas the TN1 and TN2 patients only developed detectable metastases in the lungs and/or lymph nodes (Table S1), no metastasis was detected in the brain, liver, bones, or spleen in our mouse models, as determined by BLI (Fig. S7*C*). Surprisingly, after tail-vein injection of dissociated TN1 lung metastasis-derived breast tumor cells, we observed different patterns of homing, with most of the cells homed to the spleen, liver, or bones (Fig. S7*D*), which were not spontaneous metastatic sites. In agreement with other orthotopic injection models, these observations suggest that cells injected into the tail vein encounter conditions that lead to different fates compared with spontaneous metastases from orthotopic tumors. This result also underscores

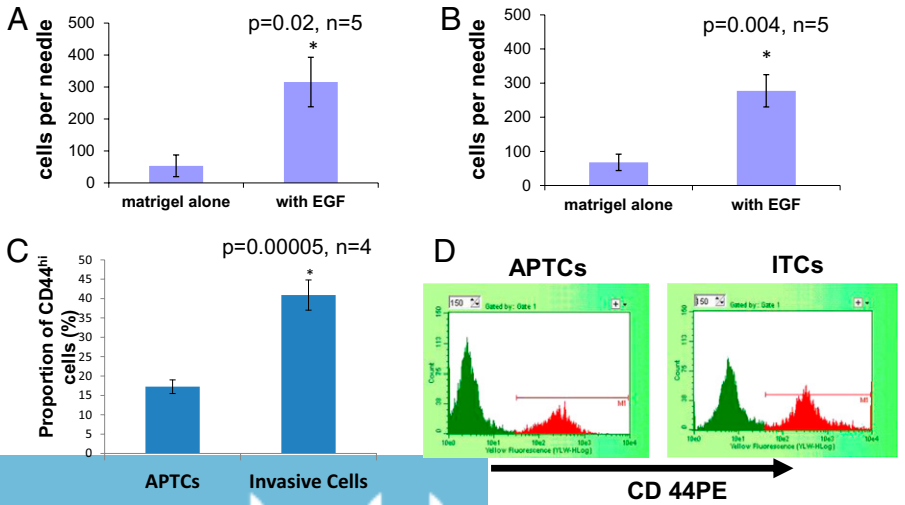

Fig. 4. Invasive cells from TN1 and TN2 breast tumors (passage 3–5) are enriched for CSC markers. (*A* and *B*) Invasive TN1 (*A*) and TN2 (*B*) cells were collected in response to human EGF (25 nmol/L), compared with Matrigel alone. Results are plotted as average number of cells per needle. Error bars represent the SEM. *A*, $*P = 0.02388$, $n = 5$; *B*, $*P = 0.00359$, $n = 5$, Student's *t* test. (*C*) Guava flow cytometry analysis of the CD44$^+$ population (percentage) contained in the APTCs and the ITCs isolated from the L2G-TN1 breast tumor. Results are shown as percentage of total GFP$^+$ cells. Error bars: SD. $*P = 0.00005$, $n = 4$. (*D*) Representative dot plot from the Guava flow cytometer analysis of CD44 expression on the TN1-APTCs and -ITCs.

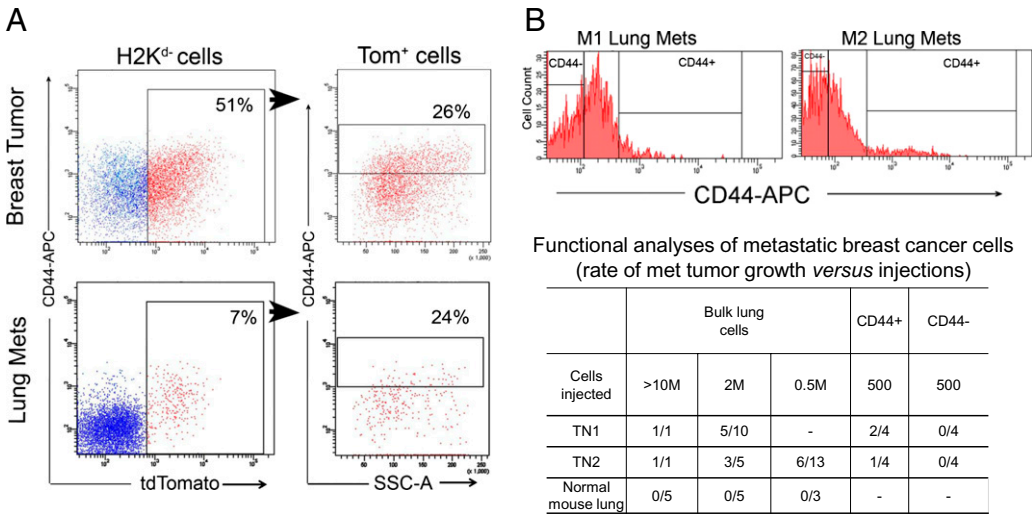

Functional analyses of metastatic breast cancer cells (rate of met tumor growth *versus* injections)

	Bulk lung cells			CD44+	CD44-
Cells injected	>10M	2M	0.5M	500	500
TN1	1/1	5/10	-	2/4	0/4
TN2	1/1	3/5	6/13	1/4	0/4
Normal mouse lung	0/5	0/5	0/3	-	-

Fig. 5. Flow cytometry analysis and tumorigenic assays of lung metastatic cancer cells. (*A*) CD44, td-Tomato, and SSC-A side scatter profiles of transduced TN2 parental breast tumor cells (*Upper*) and lung metastatic cells (*Lower*), isolated from xenografts at passage 4. (*B*) *Upper:* Flow cytometry analysis of human CD44 expression on lung metastatic cells (gated viable H2K^{d-} cells) of untransduced TN1 (passage 5) and TN2 (passage 3) tumors. The CD44^{+} and CD44^{-} gates used for sorting in tumorigenicity assays are shown. *Lower:* Table of tumorigenic assay data derived from bulk lung cells from TN1, TN2, or normal control mice as well as sorted CD44^{+} or CD44^{-} tumor cells (viable H2K^{d-} nonmouse cells). Results are shown as the number of tumors formed over the number of injections performed. These data indicate that the metastatic CSCs are enriched in CD44^{+} tumor cells.

the relevance of our model for recapitulating the metastatic cascade in human breast cancer patients.

Discussion

We have developed a robust approach for imaging of BCSC growth and dissemination, which permits both macroscopic and microscopic analysis of cancer progression. In our studies, the imaging assays facilitated development of visible human-in-mouse xenograft tumor models with spontaneous metastases to lungs or local/distant lymph nodes. Our patient-tumor derived xenograft models will be able to overcome some limitations of previous metastatic models with human cancer cell lines or mouse tumor models. Spontaneous metastases present representative features of patient tumors that can be used in predictive models of metastasis and therapeutic response, but cannot be recapitulated by lung/bone colonization models via tail-vein or intracardiac injections. This point is driven home by the observation that these xenografts metastasize to the lungs but not the bones when grown in the mammary fat pads. This likely reflects that "triple-negative" ER^{-} breast cancers tend to metastasize to the lungs rather than the bones (44). Surprisingly, when injected into the tail vein, the cells lodged at different organs, such as the bones. The molecular and cellular mechanisms underlying this phenomenon need to be further investigated. The simplest explanation is that unlike cell lines often used to study metastases, molecular pathways activated in these early-passage xenograft cells that regulate the earlier steps of metastasis (i.e., invasion and intravasation) are also obligatory for the later steps of metastasis. Our ability to collect the invasive/intravasating population of tumor cells from these TN1 and TN2 tumors will allow direct analysis of this possibility.

Traditionally, the tumorigenic assays used to identify and examine CSCs from primary tumors are labor-intensive, time-consuming (3–6 mo), and provide little or no information on the dynamics of early tumor growth or nontumorigenic cell function. With our models and noninvasive imaging, we could monitor early tumor growth and the activities of defined subsets of human breast cancer cells. The relevance of CD44^{+} CSCs function and clinical outcome has been questioned (17, 45, 46). This work further supports reports from many other groups that CD44^{+} cells correlate with EMT, unfavorable prognosis, and metastasis of clinical breast cancer (17, 20, 21, 47). In some instances, mice were injected with tumor cells at two different sites. Although it is possible that tumors grown at one flank of the recipient mice may regulate tumor cells implanted into the other flank (48), in our studies we have not observed clear regulatory (suppressive or promoting) effects, if any, of grown tumors on distant tumor cells at other injection sites of mice.

By labeling BCSCs with optical reporters, we have been able to isolate cells for further analysis or profiling. Most interestingly, our study shows that BCSCs are significantly enriched in invasive cells, suggesting that BCSC subsets are more capable of mediating invasion than non-CSCs in vivo. This implies that CD44 serve not only as markers of primary or parental BCSCs but also as markers of metastatic CSCs (MCSCs). Increased CD44 expression in invasive cells can result from both transcriptional and posttranscriptional regulations. It is not possible to determine the fate of CD44^{-} cells in lung metastasis by tail-vein injection because they bypass the invasion or intravasation steps of metastasis. Additional promoter-specific labeling of these cells may assist in addressing this issue, although the CD44 expression levels and functions are highly regulated posttranscriptionally. We also show that a portion of metastatic cancer cells in the lungs share surface markers (CD44^{+}) and functional tumorigenic properties with parental BCSCs. Thereby our work supports a colonization role for disseminating CD44^{+} CSCs during metastasis. However, it may be possible that under pathophysiologic stimuli, the CD44^{-} breast cancer cells could undergo further genetic mutations or epigenetic events that enable them to self-renew. This requires further investigations with assistance of cell labeling approaches.

The optimized strategy for labeling BCSCs with optical reporter genes can be applied to studies with CSCs associated with other malignancies (colon cancer, brain tumor, head-and-neck cancer, leukemia, etc.) and to evaluate other putative CSC markers (e.g., CD133, ALDH1, etc.) and various behaviors of subset populations. The sensitivity of detection down to 10 cells in vivo led to improved efficiency of the tumorigenic assays that were initiated with a limited number of dissociated cancer cells. Theoretically, as few as hundreds of cells in sorted subpopulations from tumor biopsies could be labeled with L2T/L2G lentiviral vectors and subjected to analyses of growth kinetics in vivo. Future studies will aim to define CSC-specific and metastasis-regulating gene sets and their promoters, label cancer cells with optical reporters driven by such unique promoters, and thereby evaluate the gene expression dynamics in CSCs and MCSCs, as well as monitor cell–

cell interaction and cell fate and function during metastasis. Stable expression of optical reporter genes in BCSCs will also enable future intravital imaging studies of BCSC-mediated early tumor initiation, invasion, circulation, and colonization via BLI and multiphoton microscopy. For these purposes, imaging will be an indispensible tool for revealing patterns of dissemination as well as determining the kinetics of tumor growth and spread to distant tissues after initiation with BCSCs. Such image analyses will also help to unravel the molecular mechanism underlying the dissemination of MCSCs by overexpression/knockdown of candidate players or regulators at genetic or epigenetic levels.

Therapeutic targeting of metastatic cells is the most challenging goal in clinical oncology. However, most of the molecular studies of metastatic mechanisms have been limited to human cancer cell lines and mouse models. We anticipate that our models and imaging strategies will be quite useful for preclinical therapeutic screenings and used as a guide to investigate therapies targeting CSCs in general or an individual patient's own tumor cells. We will investigate the effects of biological therapies on CSCs, along with the promise of preclinical imaging in development of effective cancer therapies—a promising translational application of this imaging approach.

Materials and Methods

Experimental details are provided in *SI Materials and Methods*, including materials and protocols, tumor cell isolation and flow cytometry analysis, tumor transplantation in mice, cloning, lentivirus production and transduction, CSC transduction, bioluminescence imaging, in vivo invasion assay, Guava flow cytometry analysis of APTCs and invasive cells, immunohistochemistry, RNA extraction and PCR amplification, and statistical analysis with two-tailed Student's *t* tests.

ACKNOWLEDGMENTS. We thank Dr. Geoffrey L. Greene for reviewing the manuscript; the members of Dr. Irving L. Weissman's laboratory for technical support; SCI^3, the small animal imaging facility at Stanford University; Edward Gilbert and others in the Stanford Pathology Department for histological services; and the animal core facility at Stanford University. This study was supported in part by National Institutes of Health (NIH) Grants U54 CA 126524 and P01 CA139490 and the Breast Cancer Research Foundation (to M.F.C.); NIH T90, Department of Defense Grant BC087695, and the Chicago Fellows Program at the University of Chicago (to H.L.); National Cancer Institute (NCI) In Vivo Cellular and Molecular Imaging Centers Grant P50 CA114747 and NIH R01 (to S.S.G.); the NCI R25T Stanford Molecular Imaging Scholars Program (to S.S.G. and J.P.); the Komen Foundation (J.P.); NCI R01 CA113395 (to A.P.); California Breast Cancer Research Program (to Y.S.); NCI U54 CA126511 (to S.G. and J.C.); the Breast Cancer Alliance (S.G.); and NCI CA 33572 and NIH Grant M01RR00043 (to G.S.).

1. Bonnet D, Dick JE (1997) Human acute myeloid leukemia is organized as a hierarchy that originates from a primitive hematopoietic cell. *Nat Med* 3:730–737.
2. Lapidot T, et al. (1994) A cell initiating human acute myeloid leukaemia after transplantation into SCID mice. *Nature* 367:645–648.
3. Al-Hajj M, Wicha MS, Benito-Hernandez A, Morrison SJ, Clarke MF (2003) Prospective identification of tumorigenic breast cancer cells. *Proc Natl Acad Sci USA* 100: 3983–3988.
4. Bao S, et al. (2006) Glioma stem cells promote radioresistance by preferential activation of the DNA damage response. *Nature* 444:756–760.
5. Cho RW, et al. (2008) Isolation and molecular characterization of cancer stem cells in MMTV-Wnt-1 murine breast tumors. *Stem Cells* 26:364–371.
6. Collins AT, Berry PA, Hyde C, Stower MJ, Maitland NJ (2005) Prospective identification of tumorigenic prostate cancer stem cells. *Cancer Res* 65:10946–10951.
7. Dalerba P, et al. (2007) Phenotypic characterization of human colorectal cancer stem cells. *Proc Natl Acad Sci USA* 104:10158–10163.
8. Fang D, et al. (2005) A tumorigenic subpopulation with stem cell properties in melanomas. *Cancer Res* 65:9328–9337.
9. Hermann PC, et al. (2007) Distinct populations of cancer stem cells determine tumor growth and metastatic activity in human pancreatic cancer. *Cell Stem Cell* 1:313–323.
10. Li C, et al. (2007) Identification of pancreatic cancer stem cells. *Cancer Res* 67: 1030–1037.
11. Ma S, et al. (2007) Identification and characterization of tumorigenic liver cancer stem/progenitor cells. *Gastroenterology* 132:2542–2556.
12. O'Brien CA, Pollett A, Gallinger S, Dick JE (2007) A human colon cancer cell capable of initiating tumour growth in immunodeficient mice. *Nature* 445:106–110.
13. Prince ME, et al. (2007) Identification of a subpopulation of cells with cancer stem cell properties in head and neck squamous cell carcinoma. *Proc Natl Acad Sci USA* 104: 973–978.
14. Ricci-Vitiani L, et al. (2007) Identification and expansion of human colon-cancer-initiating cells. *Nature* 445:111–115.
15. Singh SK, et al. (2003) Identification of a cancer stem cell in human brain tumors. *Cancer Res* 63:5821–5828.
16. Chan KS, et al. (2009) Identification, molecular characterization, clinical prognosis, and therapeutic targeting of human bladder tumor-initiating cells. *Proc Natl Acad Sci USA* 106:14016–14021.
17. Lawson JC, Blatch GL, Edkins AL (2009) Cancer stem cells in breast cancer and metastasis. *Breast Cancer Res Treat* 118:241–254.
18. Diehn M, et al. (2009) Association of reactive oxygen species levels and radioresistance in cancer stem cells. *Nature* 458:780–783.
19. Oravecz-Wilson KI, et al. (2009) Persistence of leukemia-initiating cells in a conditional knockin model of an imatinib-responsive myeloproliferative disorder. *Cancer Cell* 16: 137–148.
20. Liu R, et al. (2007) The prognostic role of a gene signature from tumorigenic breast-cancer cells. *N Engl J Med* 356:217–226.
21. Mani SA, et al. (2008) The epithelial-mesenchymal transition generates cells with properties of stem cells. *Cell* 133:704–715.
22. Shimono Y, et al. (2009) Downregulation of miRNA-200c links breast cancer stem cells with normal stem cells. *Cell* 138:592–603.
23. Chiang AC, Massagué J (2008) Molecular basis of metastasis. *N Engl J Med* 359: 2814–2823.
24. Nguyen DX, Bos PD, Massagué J (2009) Metastasis: From dissemination to organ-specific colonization. *Nat Rev Cancer* 9:274–284.
25. Padua D, Massagué J (2009) Roles of TGFbeta in metastasis. *Cell Res* 19:89–102.
26. Wyckoff JB, Segall JE, Condeelis JS (2000) The collection of the motile population of cells from a living tumor. *Cancer Res* 60:5401–5404.
27. Creusot RJ, et al. (2008) Tissue-targeted therapy of autoimmune diabetes using dendritic cells transduced to express IL-4 in NOD mice. *Clin Immunol* 127:176–187.
28. Edinger M, et al. (2003) Revealing lymphoma growth and the efficacy of immune cell therapies using in vivo bioluminescence imaging. *Blood* 101:640–648.
29. Mandl SJ, et al. (2004) Multi-modality imaging identifies key times for annexin V imaging as an early predictor of therapeutic outcome. *Mol Imaging* 3:1–8.
30. Ray P, De A, Min JJ, Tsien RY, Gambhir SS (2004) Imaging tri-fusion multimodality reporter gene expression in living subjects. *Cancer Res* 64:1323–1330.
31. Ray P, Tsien R, Gambhir SS (2007) Construction and validation of improved triple fusion reporter gene vectors for molecular imaging of living subjects. *Cancer Res* 67: 3085–3093.
32. Yaghoubi SS, Creusot RJ, Ray P, Fathman CG, Gambhir SS (2007) Multimodality imaging of T-cell hybridoma trafficking in collagen-induced arthritic mice: Image-based estimation of the number of cells accumulating in mouse paws. *J Biomed Opt* 12:064025.
33. Prescher JA, Contag CH (2010) Guided by the light: Visualizing biomolecular processes in living animals with bioluminescence. *Curr Opin Chem Biol* 14:80–89.
34. Paguio A, et al. (2005) pGL4 vectors: A new generation of luciferase reporter vectors. *Promega Notes* 89:4.
35. Shaner NC, et al. (2004) Improved monomeric red, orange and yellow fluorescent proteins derived from *Discosoma sp.* red fluorescent protein. *Nat Biotechnol* 22: 1567–1572.
36. Wang W, et al. (2007) Coordinated regulation of pathways for enhanced cell motility and chemotaxis is conserved in rat and mouse mammary tumors. *Cancer Res* 67: 3505–3511.
37. Perou CM, et al. (2000) Molecular portraits of human breast tumours. *Nature* 406: 747–752.
38. Rakha EA, Reis-Filho JS, Ellis IO (2008) Basal-like breast cancer: a critical review. *J Clin Oncol* 26:2568–2581.
39. Sørlie T, et al. (2001) Gene expression patterns of breast carcinomas distinguish tumor subclasses with clinical implications. *Proc Natl Acad Sci USA* 98:10869–10874.
40. Sorlie T, et al. (2003) Repeated observation of breast tumor subtypes in independent gene expression data sets. *Proc Natl Acad Sci USA* 100:8418–8423.
41. Zhao H, et al. (2004) Different gene expression patterns in invasive lobular and ductal carcinomas of the breast. *Mol Biol Cell* 15:2523–2536.
42. Bosch A, Eroles P, Zaragoza R, Viña JR, Lluch A (2010) Triple-negative breast cancer: Molecular features, pathogenesis, treatment and current lines of research. *Cancer Treat Rev* 36:206–215.
43. Contag CH, Jenkins D, Contag PR, Negrin RS (2000) Use of reporter genes for optical measurements of neoplastic disease in vivo. *Neoplasia* 2:41–52.
44. Dent R, et al. (2009) Pattern of metastatic spread in triple-negative breast cancer. *Breast Cancer Res Treat* 115:423–428.
45. Abraham BK, et al. (2005) Prevalence of CD44+/CD24-/low cells in breast cancer may not be associated with clinical outcome but may favor distant metastasis. *Clin Cancer Res* 11:1154–1159.
46. Ginestier C, et al. (2007) ALDH1 is a marker of normal and malignant human mammary stem cells and a predictor of poor clinical outcome. *Cell Stem Cell* 1:555–567.
47. Giatromanolaki A, Sivridis E, Fiska A, Koukourakis MI (2010) The CD44+/CD24- phenotype relates to 'triple-negative' state and unfavorable prognosis in breast cancer patients. *Med Oncol*, 10.1007/s12032-010-9530-3.
48. McAllister SS, et al. (2008) Systemic endocrine instigation of indolent tumor growth requires osteopontin. *Cell* 133:994–1005.